J. Math. Biol. (2014) 68:1199–1224
DOI 10.1007/s00285-013-0665-7

Mathematical Biology

# A general reaction–diffusion model of acidity in cancer invasion

**Jessica B. McGillen · Eamonn A. Gaffney · Natasha K. Martin · Philip K. Maini**

Received: 30 July 2012 / Revised: 10 January 2013 / Published online: 28 March 2013


**Abstract** We model the metabolism and behaviour of a developing cancer tumour in the context of its microenvironment, with the aim of elucidating the consequences of altered energy metabolism. Of particular interest is the Warburg Effect, a widespread preference in tumours for cytosolic glycolysis rather than oxidative phosphorylation for glucose breakdown, as yet incompletely understood. We examine a candidate explanation for the prevalence of the Warburg Effect in tumours, the acid-mediated invasion hypothesis, by generalising a canonical non-linear reaction–diffusion model of acid-mediated tumour invasion to consider additional biological features of potential importance. We apply both numerical methods and a non-standard asymptotic analysis in a travelling wave framework to obtain an explicit understanding of the range of tumour behaviours produced by the model and how fundamental parameters govern the speed and shape of invading tumour waves. Comparison with conclusions drawn under the original system—a special case of our generalised system—allows us to comment on the structural stability and predictive power of the modelling framework.

**Keywords** Cancer · Acid-mediated tumour invasion · Reaction–diffusion equations · Asymptotic analysis · Travelling waves · Numerical simulations

J. B. McGillen · E. A. Gaffney · P. K. Maini (✉)
Centre for Mathematical Biology, Mathematical Institute, Oxford University,
24-29 St Giles', Oxford OX1 3LB, UK
e-mail: maini@maths.ox.ac.uk

N. K. Martin
Department of Social Medicine, University of Bristol, Canynge Hall,
39 Whatley Road, Bristol BS8 2PS, UK

N. K. Martin
Department of Global Health and Development, London School of Hygiene
and Tropical Medicine, Keppel Street, London WCIE 7HT, UK

**Mathematics Subject Classification (2000)** 35C20 · 35K55 · 35K57 · 35Q80 · 65M20 · 92C50

## 1 Introduction

Altered energy metabolism is a near-universal feature of solid cancer tumours, and has emerged in recent years as a possible phenotypic hallmark (Hanahan and Weinberg 2011) and avenue for novel treatment strategies (Kroemer and Pouyssegur 2008). The principle of altered metabolism in tumours dates back to the seminal work of Otto Warburg (Warburg 1930). Warburg observed that rat and human carcinomas underwent glucose metabolism not by oxidative phosphorylation as in normal cells, but primarily by glycolysis, a truncated extramitochondrial pathway which produces lactic acid as a byproduct and is usually reserved for conditions of hypoxia. Although many tumour cells are subject to chronic or transient hypoxia due to crowding and faulty vasculature (Gatenby et al. 2007; Basanta et al. 2010; Gillies and Gatenby 2007), Warburg noted that tumours maintained the glycolytic pathway even when presented with sufficient oxygen for oxidative phosphorylation, indicating that the metabolic shift from oxidative phosphorylation to glycolysis—now called the Warburg Effect or glycolytic phenotype—was a fundamental change in tumour metabolism (Warburg 1956).

The intervening decades have borne out Warburg's observations. The glycolytic phenotype is sufficiently prevalent, for example, for the success of $^{18}$fluoro-2-deoxyglucose positron emission tomography (FDG-PET) imaging, which exploits the dramatically increased rate of glucose uptake exhibited by tumours expressing the glycolytic phenotype (Nieweg et al. 1996). The underlying drivers of the Warburg Effect remain largely mysterious, however, as it comes with a significant drop in absolute ATP yield per molecule of glucose compared to the normal oxidation pathway and generates a toxic lactic acid load. Possibly, uncoupling glycolysis from respiration enables tumour cells to optimise their catabolic and anabolic pathways for the rapid biosynthesis required by a programme of intensive growth (DeBerardinis et al. 2008; McCarthy 2009). Alternatively, or perhaps in complement, by acquiring resistance to acidification of the microenvironment, tumour cells expressing the glycolytic phenotype may gain a selective advantage over neighbouring, acid-sensitive, healthy cells that enables them to invade the microenvironment (Gatenby and Gillies 2004). This idea, termed the acid-mediated invasion hypothesis, is the focus of this paper.

The acid-mediated invasion hypothesis is motivated by viewing a tumour as an invasive species experiencing increasingly harsh selective pressures and undergoing somatic evolution within the microenvironment of a healthy population (Pienta et al. 2008; Clarke et al. 1990; Kallinowski et al. 1988; Vogelstein et al. 1988; Gatenby 1991; Fidler and Hart 1982; Nowell 1976); hence, it is amenable to mathematical representation as a reaction–diffusion system at the tissue scale. While many mathematical models have been developed to explore the relationships between tumour invasion, tissue acidity, and cellular metabolism and energy requirements (Smallbone et al. 2005; Venkatasubramanian et al. 2006; Bianchini and Fasano 2009; Bertuzzi et al. 2010), Gatenby and Gawlinski were the first to put the acid-mediated invasion hypothesis into a reaction–diffusion framework (Gatenby and Gawlinski 1996). Operating under

the assumption that the tumours under consideration were already expressing the Warburg Effect—that is, tumour metabolism was uncoupled from oxygen supply—the authors isolated the consequences of the glycolytic phenotype for invasion at the interface between the growing tumour and the surrounding healthy tissue. Their resulting system of non-linear partial differential equations is detailed fully in Gatenby and Gawlinski (1996), but for convenience we reproduce the equations here, with $U(X, T)$ denoting the density of healthy cells (a function of the spatial variable $X$ in units of centimetres and time $T$, measured in seconds), $V(X, T)$ the density of tumour cells, and $W(X, T)$ the concentration of extracellular lactic acid in excess of normal tissue acid concentrations. The Gatenby–Gawlinski equations (Gatenby and Gawlinski 1996) are:

$$\frac{\partial U}{\partial T} = \underbrace{\rho_1 U\left(1 - \frac{U}{\kappa_1}\right)}_{\text{logistic growth}} - \underbrace{\delta_1 U W}_{\substack{\text{acid-}\\ \text{mediated}\\ \text{healthy}\\ \text{cell death}}} \tag{1}$$

$$\frac{\partial V}{\partial T} = \underbrace{\rho_2 V\left(1 - \frac{V}{\kappa_2}\right)}_{\text{logistic growth}} + \underbrace{\frac{\partial}{\partial X}\left[\Delta_2\left(1 - \frac{U}{\kappa_1}\right)\frac{\partial V}{\partial X}\right]}_{\substack{\text{density-limited tumour}\\ \text{cell diffusion}}} \tag{2}$$

$$\frac{\partial W}{\partial T} = \underbrace{\rho_3 V - \delta_3 W}_{\substack{\text{acid production}\\ \text{by tumour cells}\\ \text{and clearance}\\ \text{by vasculature}}} + \underbrace{\Delta_3 \frac{\partial^2 W}{\partial X^2}}_{\substack{\text{chemical}\\ \text{diffusion}\\ \text{of excess}\\ \text{acid}}}. \tag{3}$$

Here the subscript '1' represents parameter association with healthy cells, '2' with tumour cells, and '3' with excess extracellular lactic acid. The constants $\kappa_{1,2}$ represent the tissue carrying capacities, $\delta_1$ the rate of acid-mediated healthy cell death, $\delta_3$ the rate of clearance of excess acid by combined buffering and vascular evacuation, $\rho_{1,2}$ the cell proliferation rates, $\rho_3$ the rate of production of excess acid by tumour cells, $\Delta_2$ the free-space diffusion coefficient of tumour cells, and $\Delta_3$ the chemical diffusion coefficient of excess acid. A key feature of this model is the density-limited tumour diffusion term in Eq. (2), the idea being that a healthy tissue operating at full carrying capacity will spatially constrain a tumour unless diminished. In Gatenby and Gawlinski (1996), numerical solution of Eqs. (1)–(3) captured two types of behaviour: invasion by a heterogeneous tumour consisting of both healthy and malignant cells, and invasion by a homogeneous tumour killing all healthy cells behind its leading edge. Further, for sufficiently aggressive tumours the authors predicted the opening of an interstitial gap between advancing malignant cells and regressing healthy cells, a previously unreported behaviour, and went on to detect gaps in fixed and flash-frozen head and neck specimens of human squamous cell carcinomas. This prediction and subsequent detection of the interstitial gap has been recognised as an elegant illustration of the benefits of a hybrid mathematical and experimental approach to the study of cancer (Byrne 2010), and the gap could, perhaps, have diagnostic potential as a marker for aggressive tumours.

The Gatenby–Gawlinski model is one of a number of studies suggesting that acidity may play an important role in tumour progression (Gillies et al. 2012). If true, this could lead to novel therapeutic strategies. One such treatment currently in development—buffering therapy—was motivated by the modelling conclusions in Gatenby and Gawlinski (1996) and aims to strip a developing tumour of its selective advantage by neutralising the pH of the microenvironment (Robey et al. 2009; Silva et al. 2009; Martin et al. 2010, 2011; Alfarouk et al. 2011; Robey and Martin 2011). In this paper we aim to further our understanding of acid-mediated invasion by generalising the Gatenby–Gawlinski model from the highly aggressive special cases considered in Gatenby and Gawlinski (1996) to capture a wider range of tumour behaviours which may be clinically relevant. In the following section (Sect. 2) we augment Eqs. (1)–(3) with biologically motivated terms. We then look both numerically (Sect. 3) and analytically (Sect. 4) into the tumour behaviours captured by this extended model, and also examine the parameter conditions governing the occurrence of interstitial gaps, as these were considered an important feature of the Gatenby–Gawlinski formulation.

## 2 Development of the generalised model

To generalise the Gatenby–Gawlinski model and explore the sensitivity of the modelling framework to the inclusion of more biological information, we incorporate two new elements. First, we add terms representing mutual competition between healthy and tumour cells for resources needed for growth, which may be postulated to be a relevant feature of the tumour–host interface where the two cell types are in close proximity. Second, we conjecture that it is biologically realistic to add a term for acid-mediated tumour cell death, as tumours are rarely observed at a pH more acidic than 6.3 (Casciari et al. 1992; Park et al. 1999) and so would not exhibit complete acid resistance. Retaining the notation used for Eqs. (1)–(3), our reaction–diffusion PDEs are:

$$\frac{\partial U}{\partial T} = \underbrace{\rho_1 U\left(1 - \frac{U}{\kappa_1} - \alpha_2\frac{V}{\kappa_1}\right)}_{\substack{\text{logistic growth with}\\ \text{cellular competition}}} - \underbrace{\delta_1 U W}_{\substack{\text{acid-}\\ \text{mediated}\\ \text{healthy}\\ \text{cell death}}} \tag{4}$$

$$\frac{\partial V}{\partial T} = \underbrace{\rho_2 V\left(1 - \frac{V}{\kappa_2} - \alpha_1\frac{U}{\kappa_2}\right)}_{\substack{\text{logistic growth with}\\ \text{cellular competition}}} - \underbrace{\delta_2 V W}_{\substack{\text{acid-}\\ \text{mediated}\\ \text{tumour}\\ \text{cell death}}} + \underbrace{\frac{\partial}{\partial X}\left[\Delta_2\left(1 - \frac{U}{\kappa_1}\right)\frac{\partial V}{\partial X}\right]}_{\substack{\text{density-limited tumour}\\ \text{cell diffusion}}} \tag{5}$$

$$\frac{\partial W}{\partial T} = \underbrace{\rho_3 V - \delta_3 W}_{\substack{\text{acid production}\\ \text{by tumour cells}\\ \text{and clearance}\\ \text{by vasculature}}} + \underbrace{\Delta_3\frac{\partial^2 W}{\partial X^2}}_{\substack{\text{chemical}\\ \text{diffusion}\\ \text{of excess}\\ \text{acid}}}. \tag{6}$$

In these equations, terms repeated from Eqs. (1)–(3) carry the same meanings as before, but now $\delta_2$ represents the rate of acid-mediated tumour cell death and $\alpha_{1,2}$ the

**Table 1** Dimensional parameter values for Eqs. (4)–(6)

| Parameter | Value | Units | Source |
|---|---|---|---|
| $\rho_1$ | $1 \times 10^{-6}$ | $s^{-1}$ | Gatenby and Gawlinski (1996) |
| $\rho_2$ | $1 \times 10^{-6}$ | $s^{-1}$ | Gatenby and Gawlinski (1996) |
| $\rho_3$ | $2.2 \times 10^{-17}$ | $cm^3 s^{-1} M$ | Martin and Jain (1994) |
| $\delta_1$ | $\mathcal{O}(1)$ | $M^{-1} s^{-1}$ | Gatenby and Gawlinski (1996) |
| $\delta_2$ | $\mathcal{O}(1)$ | $M^{-1} s^{-1}$ | Chosen to be $\mathcal{O}(\delta_1)$ |
| $\delta_3$ | $\mathcal{O}(10^{-4})$ | $s^{-1}$ | Gatenby and Gawlinski (1996) |
| $\kappa_1$ | $5 \times 10^7$ | $cm^{-3}$ | Tracqui et al. (1995) |
| $\kappa_2$ | $5 \times 10^7$ | $cm^{-3}$ | Tracqui et al. (1995) |
| $\Delta_2$ | $2 \times 10^{-10}$ | $cm^2 s^{-1}$ | Dale et al. (1994) |
| $\Delta_3$ | $5 \times 10^{-6}$ | $cm^2 s^{-1}$ | Lide (1994) |
| $\alpha_1$ | $\mathcal{O}(1)$ | Dimensionless | Chosen freely |
| $\alpha_2$ | $\mathcal{O}(1)$ | Dimensionless | Chosen freely |

relative competitive strengths of the two cell types. Values and, where appropriate, order-of-magnitude estimates for our dimensional parameters are listed in Table 1.

Letting $u = \frac{U}{\kappa_1}$, $v = \frac{V}{\kappa_2}$, $w = \frac{\delta_3 W}{\rho_3 \kappa_2}$, $t = \rho_1 T$, and $x = \sqrt{\frac{\rho_1}{\Delta_3}} X$ in Eqs. (4)–(6) produces the non-dimensionalised system

$$u_t = u(1 - u - a_2 v) - d_1 u w \tag{7}$$

$$v_t = r_2 v(1 - v - a_1 u) - d_2 v w + D[(1 - u) v_x]_x \tag{8}$$

$$w_t = c(v - w) + w_{xx} \tag{9}$$

where $a_{1,2} = \alpha_{1,2}$, $r_2 = \frac{\rho_2}{\rho_1}$, $d_{1,2} = \frac{\delta_{1,2} \rho_3 \kappa_2}{\rho_1 \delta_3}$, $c = \frac{\delta_3}{\rho_1}$, and $D = \frac{\Delta_2}{\Delta_3}$. While Eqs. (4)–(6) allow for a choice of scaling different from the one presented here—for example, a scaling which retains the rates of tumour acid production ($\rho_3$) and acid-mediated tumour cell death ($\delta_2$) as independent parameters—we employ the same non-dimensionalisation as that in Gatenby and Gawlinski (1996) to facilitate later comparisons with the Gatenby–Gawlinski model, now a special case of our generalised model. Values, order-of-magnitude estimates, and some biologically motivated constraints for our non-dimensional parameters are listed in Table 2. Importantly, for the duration of this work we require that $d_2 \leq d_1$ to capture tumour capacity for acid resistance. The Gatenby–Gawlinski model is then the limiting case of complete tumour resistance to acid, for which $d_2 = 0$ (and competition is negligible), with the other extreme being a tumour that lacks any resistance to acid ($d_2 = d_1$).

After non-dimensionalisation, the spatial domain extends along a one-dimensional ray from the tumour core at $x = -1$ out into the bulk healthy tissue at $x = 1$. We impose homogeneous Neumann boundary conditions at both spatial boundaries, $x = -1$ and $x = 1$, and initial conditions as depicted in Fig. 1, with a piece-wise linear decreasing tumour density extending out from the core and attaining zero within the domain, an analogous but reflected healthy density, and no excess extracellular acid. These boundary and initial conditions are appropriate for a travelling wave framework,

**Table 2** Table of non-dimensionalised parameter estimates for all numerical solutions of Eqs. (7)–(9) carried out in this paper.

| Parameter | Value or range | Constraint | Derivation |
|---|---|---|---|
| $r_2$ | 1 | | $\rho_2/\rho_1$ |
| $d_{1,2}$ | $\mathcal{O}(1)$ to $\mathcal{O}(10)$ | $d_2 \leq d_1$ | $\delta_{1,2} \cdot (\rho_3\kappa_2)/(\rho_1\delta_3)$ |
| $c$ | $\mathcal{O}(1)$ to $\mathcal{O}(10)$ | | $\delta_3/\rho_1$ |
| $D$ | $4 \times 10^{-5}$ | | $\Delta_2/\Delta_3$ |
| $a_{1,2}$ | $\mathcal{O}(1)$ | $a_1 \neq a_2$ | $\alpha_{1,2}$ |

In an absolute sense all parameters are order-of-magnitude estimates due to between-tumour differences and intrinsic experimental error (Fasano et al. 2009), but for our purposes we allow more variation in some parameters than others. Beyond all parameters being non-negative, we impose the constraint that $d_2 \leq d_1$ to capture tumour capacity for acid resistance, and additionally require that $a_1 \neq a_2$ as tumour and healthy cells are unlikely to consume resources with precisely the same efficiency. We do not otherwise immediately restrict $a_1$ and $a_2$ as we wish to allow for the possibility of a tumour consuming resources more aggressively ($a_2 > a_1$) or experiencing a cost of acid resistance ($a_2 < a_1$ in cases of low $d_2$)

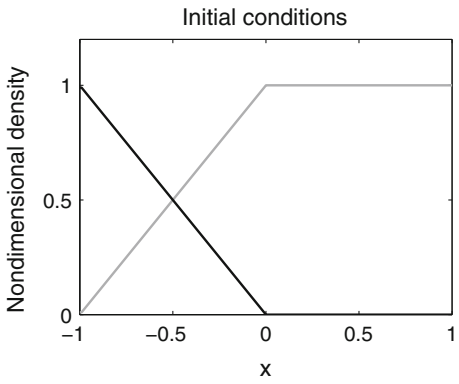


**Fig. 1** Initial conditions for the non-dimensional tumour density, $v$ (*black*), and healthy tissue density, $u$ (*grey*), in all numerical simulations of Eqs. (7)–(9). This imposes a tumour-only population at carrying capacity occupying the left-hand portion of the domain, representing the tumour core, and a healthy-only population at carrying capacity far to the right of the core. No excess acid ($w$) is present initially

to be discussed in Sect. 4, in which the tumour evolves from an invaded state in the core toward a homogeneous healthy state far from the core.

Examining our system under spatial and temporal invariance indicates the attainable types of tumour behaviour as governed by the model parameters. Equations (7)–(9) exhibit four equilibrium points, as did the original Gatenby–Gawlinski system (see Gatenby and Gawlinski 1996 for details), but whereas the healthy state was globally unstable in the Gatenby–Gawlinski formulation, leading exclusively to invasive behaviours, it is now conditionally stable in our formulation, allowing both invasive and non-invasive behaviours. The stationary points for Eqs. (7)–(9) are:

1. a trivial absence of all species, $(u, v, w) = (0, 0, 0)$, globally unstable;
2. a healthy state, $(u, v, w) = (1, 0, 0)$, linearly unstable if $a_1 < 1$ and stable if $a_1 > 1$;
3. a heterogeneous state, $(u, v, w) = (1 - (a_2 + d_1)\tilde{v}, \tilde{v}, \tilde{v})$,
   where $\tilde{v} = \dfrac{1 - a_1}{1 - a_1 a_2 + \frac{d_2}{r_2} - a_1 d_1}$,
   linearly unstable if $d_1 > 1 + \frac{d_2}{r_2} - a_2$ and stable if $0 < d_1 < 1 + \frac{d_2}{r_2} - a_2$; and

4. a homogeneous tumour state, $(u, v, w) = \left(0, \frac{1}{1+\frac{d_2}{r_2}}, \frac{1}{1+\frac{d_2}{r_2}}\right)$,
linearly unstable if $0 < d_1 < 1 + \frac{d_2}{r_2} - a_2$ and stable if $d_1 > 1 + \frac{d_2}{r_2} - a_2$,

noting again that we always require $d_2 \leq d_1$ to capture tumour capacity for acid resistance. In combination with the initial conditions we impose on the system (Fig. 1) these steady states and their stability lead to various tumour behaviours which we explore numerically in the following section.

## 3 Numerical exploration of the generalised model

Our initial conditions (Fig. 1) impose a tumour-only state at $x = -1$ and a healthy-only state at $x = 1$, and we expect the system to evolve over time according to the analysis in Sect. 2, producing four types of tumour behaviour. If $a_1 < 1$, then the healthy state is unstable and we expect the tumour to propagate in the positive $x$-direction, establishing behind the moving tumour-healthy interface either a heterogeneous state with both cell types coexisting at reduced densities, if $0 < d_1 < 1 + d_2/r_2 - a_2$, or a homogeneous tumour state if $d_1 > 1 + d_2/r_2 - a_2 > 0$. If $a_1 > 1$, then we expect the stable healthy state to prevent tumour invasion, instead either clearing the tumour if $0 < d_1 < 1 + d_2/r_2 - a_2$ or establishing a stationary interface with the stable tumour population if $d_1 > 1 + d_2/r_2 - a_2$. In all cases we additionally require that $d_2 \leq d_1$, to capture tumour capacity for resistance to acid.

We solve Eqs. (7)–(9) numerically in Matlab using the Method of Lines (Schiesser 1991), with the system of partial differential equations discretised using a spatial step of $\mathrm{d}x = 0.005$ and the resulting system of linked ordinary differential equations solved through time using Matlab's inbuilt ODE15s algorithm to accommodate stiffness. All simulations are run to at least $t = 20$, corresponding to approximately 0.6 years, to ensure complete decay of transients, and initial and boundary conditions are imposed as described in Sect. 2. The particular initial configuration shown in Fig. 1 is chosen simply for clear delineation of tumour vs. healthy tissue, with the interface positioned at the domain midpoint ($x = 0$) to allow enough space in the domain for us to observe either leftward- or rightward-propagating waves. Changing the initial conditions (not shown) does not alter the overall system behaviour, provided the biologically-motivated boundary constraints are met; that is, one end of the domain (here $x = -1$) is primarily tumour, and the other end (here $x = 1$) is exclusively healthy tissue. The wavespeed of an invasive tumour—here, one that propagates in the positive $x$-direction—is measured by tracking the midpoint of the front as it evolves near the end of each simulation.

The accuracy of our numerical method is confirmed by setting $a_1 = a_2 = d_2 = 0$ in Eqs. (7)–(9) to recover the two behaviours captured by the Gatenby–Gawlinski model, heterogeneous invasion and homogeneous invasion, with wavespeeds closely matching those measured in Gatenby and Gawlinski (1996) (Fig. 2). Additionally, upon setting $d_1 = d_2 = 0$ in Eqs. (7)–(9) to remove acid-mediated cell death, we attain, as expected, the dynamics of a classical mutual-competition system (not shown) in

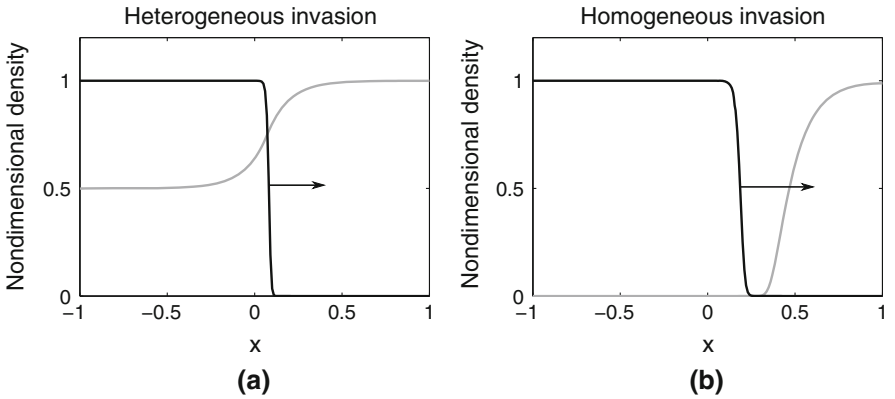


**Fig. 2** Recovery of dynamics in Gatenby and Gawlinski (1996). Profiles of tumour density (*black*) and healthy density (*grey*) from numerical simulations of Eqs. (1)–(3), non-dimensionalised and subject to the initial and boundary conditions detailed in Sect. 2, with *arrows* indicating the direction of tumour propagation. Excess extracellular acid is omitted for clarity but tracks the tumour front with a shallower profile. **a** Heterogeneous invasion is obtained by setting $d_1 = 0.5$, producing a non-dimensional wavespeed of 0.0066 (corresponding to approximately 0.01 mm/day). **b** Homogeneous invasion with an interstitial gap is obtained by setting $d_1 = 12.5$, producing a non-dimensional wavespeed of 0.0128 (approximately 0.03 mm/day). Each simulation was run to a final time of $t = 20$ (approximately 0.6 years) to ensure complete decay of transients. Other parameter values are $r_2 = 1$, $D = 4 \times 10^{-5}$, and $c = 70$

which the competition parameters, here $a_1$ and $a_2$, govern the linear stability of the system (Murray 2002).

Numerical solution of our full system, Eqs. (7)–(9) with all parameters non-zero, produces the four expected types of tumour behaviour (Fig. 3). While the two invasive types seen in Gatenby and Gawlinski (1996) are still present in our model—when $a_1 < 1$ and $d_1 < 1 + d_2/r_2 - a_2$ we see heterogeneous invasion (Fig. 3a) and when $a_1 < 1$ and $d_1 > 1 + d_2/r_2 - a_2$ we see homogeneous invasion (Fig. 3b)—we also capture two other types of behaviour. First, when $a_1 > 1$ and $d_1 > 1 + d_2/r_2 - a_2$ we see a non-aggressive tumour which appears stationary for a time (Fig. 3c). This behaviour is unlikely to persist, however, as our simulations indicate that a truly stationary outcome requires a tumour with both no acid resistance (i.e. the limiting case of $d_2 = d_1$) and a competitive strength precisely equivalent to that of the healthy cells (i.e. $1 < a_1 = a_2$); but these are biologically unlikely conditions and, in the case of the latter, dependent upon mathematical parameter fine-tuning. Instead, the delicate balance between the two stable homogeneous states will be tipped in one direction or the other by inequalities between the two populations. If the tumour has no acid resistance ($d_2 = d_1$) and the healthy population is the stronger competitor ($a_1 > a_2$) then the tumour will eventually be cleared in a manner similar to Fig. 3d; but if the tumour does exhibit acid resistance ($d_2 < d_1$), as is more plausible biologically, then it will invade. Nevertheless, the speed of invasion is extremely slow—for example, the parameter set $\{a_1, a_2, d_1, d_2\} = \{1.4, 1.6, 10, 8\}$ produces a tumour which advances by less than half a millimetre over a year of simulation time—and hence tumours in this regime, while not strictly stationary, can be considered non-aggressive, at least in comparison with the faster-moving types in the $a_1 < 1$ regimes (Fig. 3a, b) which travel

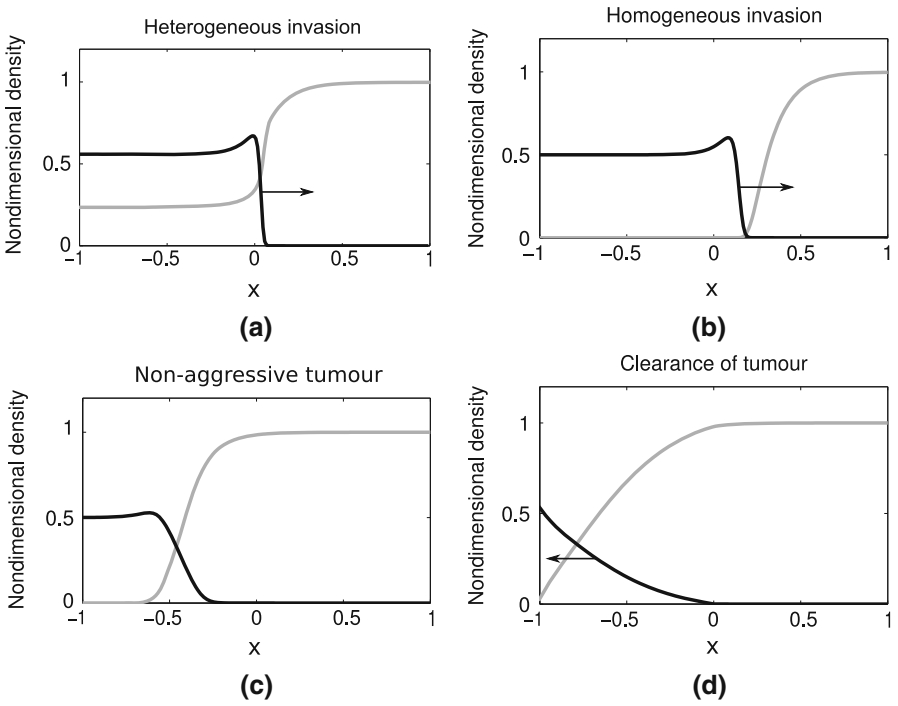


**Fig. 3** Representative time-evolving profiles of tumour density (*black*) and healthy density (*grey*) from numerical solutions of Eqs. (7)–(9) according to parameter regime, with *arrows* indicating the direction of tumour propagation. **a** Heterogeneous tumour invasion with healthy cells surviving behind the tumour-healthy interface, **b** homogeneous tumour invasion with no healthy cells remaining behind the interface, **c** establishment of a non-aggressive tumour which can progress either toward clearance, in the limiting case of no tumour acid-resistance, or toward very slow invasion, and **d** clearance of the tumour by the healthy population. Each simulation was run to a final time of $t = 20$ (approximately 0.6 years)

on the order of 4 mm per year. The final observed behaviour is truly non-invasive: when $a_1 > 1$ and $d_1 < 1 + d_2/r_2 - a_2$, the healthy cells clear away the tumour (Fig. 3d).

While the numerical exploration detailed here provides us with a high-level understanding of the attainable tumour behaviours, it does not indicate where in parameter space interstitial gaps can occur, or indeed whether they are permissible under our generalised system. Moreover, from numerical simulations alone we cannot elucidate explicitly how the system behaviours depend on fundamental model parameters; and as the parameter space is high-dimensional, an implicit description is inadequate for building a comprehensive picture of the system. Simulations do indicate, however, that in the invasive parameter regimes the system exhibits travelling tumour waves of constant velocity and shape, which arise due to propagation into the unstable healthy state (van Saarloos 1988); hence, in the following section we carry out a travelling wave analysis of Eqs. (7)–(9) to attain an explicit understanding of the dynamics. Very broadly this analysis follows the strategy taken in Fasano et al. (2009) on the Gatenby–Gawlinski system, but with the introduction of extra subtleties due to increased coupling in our more comprehensive model.

## 4 Analysis of the generalised model

We transform Eqs. (7)–(9) into travelling wave coordinates by letting, with a mild abuse of notation, $u(x,t) = u(z)$, $v(x,t) = v(z)$, and $w(x,t) = w(z)$ where $z = x - \theta t$ is our travelling wave coordinate and $\theta$ the (constant, positive) wavespeed. Extending the spatial domain to the real line to allow for travelling waves, we obtain, with $\dot{}$ denoting differentiation with respect to $z$:

$$-\theta\dot{u} = u(1-u-a_2v) - d_1uw \tag{10}$$

$$-\theta\dot{v} = D(\ddot{v}(1-u) - \dot{u}\dot{v}) + r_2v(1-v-a_1u) - d_2vw \tag{11}$$

$$-\theta\dot{w} = \ddot{w} + c(v-w). \tag{12}$$

In Eqs. (10)–(12) the wavefront is now fixed through translational invariance at $z = 0$, with $z < 0$ behind the advancing wavefront and $z > 0$ ahead. Accordingly, we impose the healthy state at the boundary far ahead of the tumour wavefront and one of the two invaded states (heterogeneous or homogeneous) far behind, such that the travelling-wave boundary conditions are:

$$(u,v,w)(\infty) = (1,0,0), \quad \text{and} \tag{13}$$

$$(u,v,w)(-\infty) = \begin{cases} (1-(a_2+d_1)\tilde{v}, \tilde{v}, \tilde{v}) & \text{if } d_1 < 1 + \dfrac{d_2}{r_2} - a_2, \text{ or} \\ \left(0, \dfrac{1}{1+\frac{d_2}{r_2}}, \dfrac{1}{1+\frac{d_2}{r_2}}\right) & \text{if } d_1 > 1 + \dfrac{d_2}{r_2} - a_2, \end{cases} \tag{14}$$

where $\tilde{v} = \dfrac{1-a_1}{1-a_1a_2+\frac{d_2}{r_2}-a_1d_1}$ as before.

In Eq. (11) the parameter $D$, the ratio between the free-space tumour and acid diffusion coefficients, is very small, and we exploit it as an asymptotically small parameter by relating it to the wavespeed via consideration of the fast and slow dynamics of Eqs. (10)–(12). That is, we let $z = x - \epsilon\theta_0 t$ where $\epsilon = \sqrt{D} \ll 1$ and $\theta_0$ is $O(1)$. The system becomes:

$$-\epsilon\theta_0\dot{u} = u(1-u-a_2v) - d_1uw \tag{15}$$

$$-\epsilon\theta_0\dot{v} = \epsilon^2(\ddot{v}(1-u) - \dot{u}\dot{v}) + r_2v(1-v-a_1u) - d_2vw \tag{16}$$

$$-\epsilon\theta_0\dot{w} = \ddot{w} + c(v-w). \tag{17}$$

It is clear from numerical simulations (for example, Fig. 3a) that the system exhibits a boundary layer: within and near the tumour wavefront is a region of rapid change for the species and their derivatives, while far behind and ahead of the wavefront the changes are much slower. To asymptotic (leading order) accuracy, the solution in the slowly-varying outer regions satisfies Eqs. (15)–(17) with $\epsilon = 0$:

$$0 = u(1 - u - a_2 v) - d_1 u w \tag{18}$$
$$0 = r_2 v(1 - v - a_1 u) - d_2 v w \tag{19}$$
$$0 = \ddot{w} + c(v - w). \tag{20}$$

Rescaling the narrow wavefront region by setting $z = \epsilon\zeta$, the leading order solution in the wavefront region satisfies, with the subscript 'in' denoting a profile in this inner region and $'$ denoting differentiation with respect to the 'stretched' inner coordinate $\zeta$,

$$-\theta_0 u'_{in} = u_{in}(1 - u_{in} - a_2 v_{in}) - d_1 u_{in} w_{in} \tag{21}$$
$$-\theta_0 v'_{in} = v''_{in}(1 - u_{in}) - u'_{in} v'_{in} + r_2 v_{in}(1 - v_{in} - a_1 u_{in}) - d_2 v_{in} w_{in} \tag{22}$$
$$w''_{in} = 0. \tag{23}$$

The Gatenby–Gawlinski model, a subset of our generalised model, exhibits interstitial gaps and sharp fronts—profiles under semi-compact support with a discontinuity in the derivative where zero density is reached—under certain parameter regimes (Fasano et al. 2009); hence, we must allow for these possibilities in our model.

We proceed by first finding an approximate solution for the healthy profile ($u$) to asymptotic accuracy, then finding an asymptotic approximation for the excess acid profile ($w$) and using both of these to determine the dynamics in the tumour wavefront.

### 4.1 Asymptotic approximation for the healthy profile, $u$

Before considering the asymptotic structure of the problem for evaluating $u$, from Eq. (15) we have exactly that

$$\dot{u} = \frac{u^2 - A(z)u}{\epsilon\theta_0}, \quad \text{where} \tag{24}$$
$$A(z) = 1 - a_2 v - d_1 w \tag{25}$$

and $A(+\infty) = 1$. In the outer regions this will invoke a fast relaxation to one of the roots, $u = 0$ or $u = A(z)$, and in the inner region the $u$ derivatives are larger still, so the same behaviour will occur; hence to asymptotic accuracy we expect to have $u \approx 0$ or $u \approx A(z)$, as follows.

With the substitution $u = 1/q$, Eq. (24) becomes

$$\epsilon\theta_0 \dot{q} = A(z)q - 1,$$

a linear equation which we solve directly to obtain

$$q(z) = e^{-\frac{1}{\epsilon\theta_0}\int_z^{\tilde{z}} A(s)ds} q(\tilde{z}) + \frac{1}{\epsilon\theta_0} e^{\frac{1}{\epsilon\theta_0}\int_0^z A(s)ds} \int_z^{\tilde{z}} e^{-\frac{1}{\epsilon\theta_0}\int_0^s A(x)dx} ds$$

where $\tilde{z}$ is a judicious choice of $z$. Choosing this $\tilde{z}$ to be extremely large, but not infinite since $\int_z^\infty A(s)ds$ is ill-defined, we have $q(\tilde{z}) = 1/u(\tilde{z}) \approx 1$ because of the healthy-state boundary conditions imposed on $u(z)$ as $z \to +\infty$. Substituting $u(z)$ back into the equation, we obtain

$$u(z) \approx \frac{e^{\frac{1}{\epsilon\theta_0}\int_z^{\tilde{z}} A(s)ds}}{1 + \frac{1}{\epsilon\theta_0} e^{\frac{1}{\epsilon\theta_0}\int_0^{\tilde{z}} A(s)ds} \int_z^{\tilde{z}} e^{-\frac{1}{\epsilon\theta_0}\int_0^s A(x)dx} ds},$$

and with

$$\phi(s) = -\frac{1}{\theta_0}\int_0^s A(x)dx \quad \text{and}$$

$$I(z) = \int_z^{\tilde{z}} e^{\frac{1}{\epsilon}\phi(s)} ds$$

this becomes

$$u(z) \approx \frac{e^{\frac{1}{\epsilon\theta_0}\int_z^{\tilde{z}} A(s)ds}}{1 + \frac{I(z)}{\epsilon\theta_0} e^{\frac{1}{\epsilon\theta_0}\int_0^{\tilde{z}} A(s)ds}} \tag{26}$$

where $I(z)$ is a Laplace integral (Bender and Orszag 1999).

These expressions implicitly assume that $u \approx \max\{0, A(z)\}$ is such that $A(z) = 1 - a_2 v - d_1 w$ has at most one root. Ahead of the wavefront, $v \approx 0$ and hence $A(z) = 1 - d_1 w$, which is increasing as $w$ always decreases (this is evident from numerical solutions and also will be seen in Sect. 4.2); thus there can be at most one root ahead of the wavefront. This root is illustrated by Case 1c of Fig. 4, which depicts the possible locations of the tumour wavefront in relation to the zeros of $A(z)$. Considering two or three roots, as illustrated in the third and fourth rows of Fig. 4, respectively, we immediately have an absence of monotonicity in $u$ which is not consistent with our numerical results. Furthermore, Case 1b in Fig. 4 requires parameter fine tuning, and hence we do not consider it, in view of the variability in our parameters imparted by between-tumour variation and intrinsic experimental error (Fasano et al. 2009). We are left with Cases 0a, 1a, or 1c from Fig. 4, which we explore below.

For fixed $z$, suppose that $A > 0$ on the interval $[z, \tilde{z}]$, with $\tilde{z} \gg 1$, and hence has no roots; this is Case 0 in Fig. 4. Then we have that $\dot{\phi}(s) = -\frac{1}{\theta_0} A(s) < 0$ for all $s$ in $[z, \tilde{z}]$, indicating that on the interval $[z, \tilde{z}]$, $\frac{1}{\epsilon}\phi(s)$ has its maximum at $s = z$, and we Taylor expand $I(z)$ about this point:

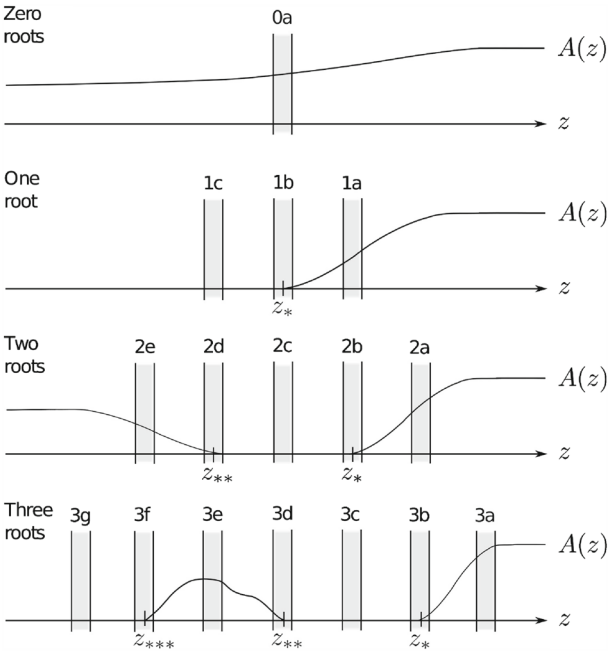


**Fig. 4** Locations along $z$ where the inner wavefront region can fall (*shaded columns*) in relation to the roots of $A(z)$, the function given by Eq. (25) and shown as a *black curve*, for four possible scenarios: no roots (*top*), a single root at $z_*$ (*second from top*), two roots at $z_*$ and $z_{**}$ (*second from bottom*), or three roots at $z_*$, $z_{**}$, and $z_{***}$ (*bottom*)

$$\begin{aligned} I(z) &\approx \int_z^{\tilde{z}} e^{\frac{1}{\epsilon}[\phi(z)+(s-z)\dot{\phi}(z)]} ds \\ &\approx -\frac{\epsilon}{\dot{\phi}(z)} e^{\frac{1}{\epsilon}\phi(z)} \end{aligned}$$

where the second line follows from the first by extension of the upper limit of integration to $\infty$ in accordance with the Laplace Method (Bender and Orszag 1999), introducing only exponentially small errors. Substituting this into Eq. (26), we obtain

$$\begin{aligned} u(z) &\approx \frac{e^{\frac{1}{\epsilon\theta_0}\int_z^{\tilde{z}} A(s)ds}}{1+\frac{1}{A(z)}e^{\frac{1}{\epsilon\theta_0}\int_z^{\tilde{z}} A(s)ds}} \\ &\approx \frac{e^{\frac{1}{\epsilon\theta_0}\int_z^{\tilde{z}} A(s)ds}}{\frac{1}{A(z)}e^{\frac{1}{\epsilon\theta_0}\int_z^{\tilde{z}} A(s)ds}} \\ &= A(z) \end{aligned}$$

with the second line following from the first by the observation that $A(s) > 0$ for all $s$ in $\left[z, \tilde{z}\right]$ and hence the exponential dominates unity.

If $A(s)$ has one root at $s = z_*$, then for $z > z_*$ the asymptotics are analogous to the no-root case and $u \approx A(z)$; here we consider $z < z_*$, corresponding to Case 1a or 1c in Fig. 4. We have at $z_*$ that $\dot{\phi}(z_*) = -\frac{1}{\theta_0}A(z_*) = 0$, and it follows that $\ddot{\phi}(z_*) = -\frac{1}{\theta_0}A'(z_*) \leq 0$. Excluding the mathematically fine-tuned degenerate case for which $\ddot{\phi}(z_*) = 0$, we assume that $\ddot{\phi}(z_*) < 0$ and expand $I(z)$ about $s = z_*$:

$$\begin{aligned} I(z) &\approx \int_z^{\tilde{z}} e^{\frac{1}{\epsilon}\left[\phi(z_*)+\frac{(s-z_*)^2}{2}\ddot{\phi}(z_*)\right]}ds \\ &\approx e^{\frac{1}{\epsilon}\phi(z_*)}\sqrt{\frac{2\pi\epsilon}{-\ddot{\phi}(z_*)}} \end{aligned}$$

with the second line following from the first by extension of the limits of integration to $-\infty$ and $+\infty$, again introducing only exponentially small errors. Substituting this into Eq. (26) gives us

$$\begin{aligned} u(z) &\approx \frac{e^{\frac{1}{\epsilon\theta_0}\int_z^{\tilde{z}} A(s)ds}}{1+\frac{1}{\epsilon\theta_0}e^{\frac{1}{\epsilon\theta_0}\int_{z_*}^{\tilde{z}} A(s)ds}\sqrt{\frac{2\pi\epsilon\theta_0}{\dot{A}(z_*)}}} \\ &\approx \frac{e^{\frac{1}{\epsilon\theta_0}\int_z^{\tilde{z}} A(s)ds}}{\frac{1}{\epsilon\theta_0}e^{\frac{1}{\epsilon\theta_0}\int_{z_*}^{\tilde{z}} A(s)ds}\sqrt{\frac{2\pi\epsilon\theta_0}{\dot{A}(z_*)}}} \\ &= \sqrt{\frac{\epsilon\theta_0\dot{A}(z_*)}{2\pi}}e^{\frac{1}{\epsilon\theta_0}\int_z^{z_*} A(s)ds} \\ &\approx 0 \end{aligned}$$

where the final line comes from letting $\epsilon \to 0$ for an approximation to leading order in $\epsilon$, noting that in the interval from $z$ to $z_*$ we have $A(s) < 0$ and hence the exponential vanishes.

Consistent with our initial expectation, we have found that

$$u \approx \max\{0, A(z)\} \tag{27}$$

to leading order. In the following section we incorporate this solution into an asymptotic approximation for the excess acid profile, $w$.

### 4.2 Asymptotic approximation for the acid profile, $w$

Depending on the type of invasive behaviour as determined by the imposed boundary conditions, either heterogeneous invasion or homogeneous invasion is possible, with

the limit in $z < 0$ corresponding to the appropriate boundary condition at $z = -\infty$ from Eq. (14). Furthermore, ahead of the wavefront, Eq. (19) governs the tumour density and hence we have either $v = 1 - a_1 u - d_2 w/r_2$ or $v = 0$ to asymptotic accuracy. The former can be discounted immediately as it is inconsistent with the boundary condition at spatial infinity, except for the mathematical fine tuning $a_1 = 1$, which corresponds to the confluence of two of the steady states and is excluded by the conditions for invasion. Therefore, for invading waves we have, to asymptotic accuracy, $v = 0$ for all $z > 0$. In this region, Eq. (20) becomes $0 = \ddot{w} - cw$, and from this we find the leading-order solution for $w$ for $z$ sufficiently large:

$$w_+ = k_1 e^{-\sqrt{c}z} \tag{28}$$

where $k_1$ is to be determined. In $z < 0$ we have $0 = \ddot{w} + c(v - w)$, and the profiles in $z < 0$ then depend on invasive type as follows.

When we enforce the boundary conditions for heterogeneous invasion by requiring that $a_1 < 1$ and $d_1 < 1 + \frac{d_2}{r_2} - a_2$, for all $z < 0$ we have $v \neq 0$ and $u > 0$ everywhere; hence from Eq. (27) we have $u = A(z) > 0$ (Case 0 in Fig. 4). Under these conditions, Eq. (20) becomes

$$-\frac{c(1-a_1)}{1-a_1a_2} = \ddot{w} - c\left(1 + \frac{\frac{d_2}{r_2} - a_1 d_1}{1 - a_1 a_2}\right) w.$$

Letting

$$\lambda = 1 + \frac{\frac{d_2}{r_2} - a_1 d_1}{1 - a_1 a_2} \quad \text{and, as before,}$$
$$\tilde{v} = \frac{1 - a_1}{1 - a_1 a_2 + \frac{d_2}{r_2} - a_1 d_1},$$

solving this linear ordinary differential equation and applying the heterogeneous boundary condition for $w$ at $z = -\infty$ yields the leading-order solution for $w$,

$$w_- = k_2 e^{z\sqrt{c\lambda}} + \tilde{v},$$

for all $z < 0$. To find the unknown constants $k_1$ and $k_2$ and determine the inner solution for the acid, $w_{in}$, we match the functional forms of the leading-order approximations for $w$ in each of the outer regions with those in the inner region within the overlapping boundary regions. To leading order $w_{in}$ is given by Eq. (23); this equation could be satisfied by a linear $w_{in}$, but as $w_{in}$ must be bounded in order to match with the bounded outer regions, it must be constant rather than linear. Consequently, matching the outer solutions to the inner boundaries is equivalent to matching the functional forms of $w_-(0)$ and $w_+(0)$ with one another across the constant inner region where both take the value of $w_{in}$. We match the functions, $w_-(0) = w_+(0)$, and their derivatives, $\dot{w}_-|_0 = \dot{w}_+|_0$, to obtain at leading order in $\epsilon$:

$$w = \begin{cases} \tilde{v}\left(1 - \dfrac{e^{z\sqrt{c\lambda}}}{1+\sqrt{\lambda}}\right) & \text{for } z < 0, \\ \dfrac{\tilde{v}e^{-z\sqrt{c}}}{1+\sqrt{\frac{1}{\lambda}}} & \text{for } z > 0, \end{cases} \tag{29}$$

and it follows that for all $\zeta$,

$$w_{in} = \frac{\tilde{v}}{1+\sqrt{\frac{1}{\lambda}}} \tag{30}$$

in the heterogeneous invasion case. The sign of $\lambda$ exerts an extra constraint on our parameter space, in that $\lambda$ must be positive for solutions for $w$ to be real, and hence we must have

$$d_1 < \frac{1}{a_1}\left(1 + \frac{d_2}{r_2}\right) - a_2. \tag{31}$$

When we enforce the boundary conditions for homogeneous invasion by requiring that $a_1 < 1$ and $d_1 > 1 + \frac{d_2}{r_2} - a_2$, ahead of the wavefront we have $v \approx 0$ and the behaviour of $w$ is as previously, but in $z < 0$ the limit as $z \to -\infty$ now tends to the homogeneous boundary condition. Again we find from Eq. (20) that

$$-\frac{c(1-a_1)}{1-a_1a_2} = \ddot{w} - c\lambda w,$$

and solving this ODE, now with the homogeneous boundary condition imposed on $w$, gives

$$w_- = k_3 e^{z\sqrt{c\lambda}} + \frac{1}{1+\frac{d_2}{r_2}}$$

for $z < 0$. Matching the functional form of this solution with the solution in $z > 0$, given by Eq. (28), we obtain the outer solution for $w$ to asymptotic accuracy:

$$w = \begin{cases} \dfrac{1}{1+\frac{d_2}{r_2}}\left(1 - \dfrac{e^{z\sqrt{c\lambda}}}{1+\sqrt{\lambda}}\right) & \text{for } z < 0, \\ \dfrac{e^{-z\sqrt{c}}}{\left(1+\frac{d_2}{r_2}\right)\left(1+\sqrt{\frac{1}{\lambda}}\right)} & \text{for } z > 0, \end{cases} \tag{32}$$

and it follows that for all $\zeta$,

$$w_{in} = \frac{1}{\left(1 + \frac{d_2}{r_2}\right)\left(1 + \sqrt{\frac{1}{\lambda}}\right)} \tag{33}$$

in the homogeneous invasion case, again subject to the parameter restriction in Eq. (31). We now use the solutions from this section and Sect. 4.1 to extract the tumour wavespeed, $\theta$, from the equation governing the tumour wavefront, Eq. (22).

### 4.3 Determination of the wavespeed, $\theta$

To find the invasive speed, $\theta$, of an invading tumour wave in our system, we again consider each type of invasion—heterogeneous and homogeneous—as dictated by parameter conditions.

When $a_1 < 1$ and $d_1 < 1 + \frac{d_2}{r_2} - a_2$, leading to heterogeneous invasion, in order to match with the appropriate boundary conditions we must have from Sect. 4.1 that $u \approx A(z) > 0$ everywhere in the domain. Incorporating our solution for $w$, Eq. (30), we have

$$u_{in} \approx 1 - a_2 v_{in} - \frac{d_1 \tilde{v}}{1 + \sqrt{\frac{1}{\lambda}}}$$

to leading order in $\zeta$ in the inner region, and it follows that $u'_{in} = -a_2 v'_{in}$. With these leading-order solutions for $u_{in}$ and $w_{in}$, the asymptotic equation for the wavefront, Eq. (22), becomes

$$0 = a_2[v_{in}v'_{in}]' + \alpha v''_{in} + \theta_0 v'_{in} + v_{in}(\beta - \gamma v_{in}) \tag{34}$$

where

$$\alpha = \frac{d_1 \tilde{v}}{1 + \sqrt{\frac{1}{\lambda}}},$$

$$\beta = r_2\left(1 - a_1 - \tilde{v}\frac{\frac{d_2}{r_2} - a_1 d_1}{1 + \sqrt{\frac{1}{\lambda}}}\right), \quad \text{and}$$

$$\gamma = r_2(1 - a_1 a_2).$$

Recalling that the healthy state imposed at $z = +\infty$ is unstable, we have the type of propagation in which the wave is pulled by the instability at its leading edge (van Saarloos 1988). At this leading edge the tumour density, $v_{in}$, is very small and the degenerate term in Eq. (34), $a_2[v_{in}v'_{in}]'$, becomes negligible, allowing us to consider only

$$0 \approx \alpha v_{in}'' + \theta_0 v_{in}' + v_{in}(\beta - \gamma v_{in}),$$

which is a Fisher-type equation and by marginal stability exhibits an asymptotic front speed of $\theta_0 = 2\sqrt{\alpha\beta}$. Substituting back to the original parameters and recalling that $\theta = \epsilon\theta_0 = \sqrt{D}\theta_0$, we obtain the speed

$$\theta \approx 2\sqrt{D}\sqrt{\frac{d_1 r_2 \tilde{v}}{1+\sqrt{\frac{1}{\lambda}}}\left(1 - a_1 - \tilde{v}\frac{\frac{d_2}{r_2} - a_1 d_1}{1+\sqrt{\frac{1}{\lambda}}}\right)} \tag{35}$$

in the heterogeneous invasion case.

When $a_1 < 1$ and $d_1 > 1 + \frac{d_2}{r_2} - a_2$, leading to homogeneous invasion, to satisfy the appropriate boundary conditions we must have $u$ tending to zero somewhere in the domain; thus, $A(z)$ must have a root, and whether or not $u$ plays a role in the inner region depends on where this root is located. Using Eq. (32) and our previous argument that $v \approx 0$ in $z > 0$, we have, for all $z > 0$,

$$u \approx \max\left\{0, 1 - \frac{d_1 e^{-z\sqrt{c}}}{\left(1 + \frac{d_2}{r_2}\right)\left(1 + \sqrt{\frac{1}{\lambda}}\right)}\right\}. \tag{36}$$

The system behaviour in the wavefront now depends on whether the root of $A(z)$ falls in $z > 0$; that is, whether the magnitude of $d_1$ is sufficient to drive $u$ to zero ahead of the tumour wavefront. For notational convenience we let

$$\sigma = \left(1 + \frac{d_2}{r_2}\right)\left(1 + \sqrt{\frac{1}{\lambda}}\right).$$

If $d_1 < \sigma$, then $u$ is driven to zero in $z < 0$ by matching to the limit as $z \to -\infty$ (Case 1a from Fig. 4). We thus expect $u_{in}$ to be nonzero, resulting in homogeneous tumour invasion with no interstitial gap and the inner travelling wave equation

$$0 = \alpha v_{in}'' + \theta_0 v_{in}' + v_{in}(\beta - \gamma v_{in})$$

where

$$\alpha = \frac{d_1}{\sigma}$$
$$\beta = r_2\left(1 - a_1 - \frac{\frac{d_2}{r_2} - a_1 d_1}{\sigma}\right), \quad \text{and}$$
$$\gamma = r_2(1 - a_1 a_2).$$

It follows that the asymptotic front speed is

$$\theta \approx 2\sqrt{D}\sqrt{\frac{d_1 r_2}{\sigma}\left(1 - a_1 - \frac{\frac{d_2}{r_2} - a_1 d_1}{\sigma}\right)}. \tag{37}$$

If $d_1 = \sigma$, then $u \approx \max\{0, 1 - e^{-z\sqrt{c}}\}$, and $u$ attains zero inside the narrow inner region; this is the mathematically fine-tuned Case 1b from Fig. 4, and considering the potential variance in parameter values across tumours, we do not proceed further with it.

If $d_1 > \sigma$, then this condition is sufficient to push $u$ to zero at some $z_* > 0$ (Case 1c from Fig. 4), resulting in homogeneous invasion with an interstitial gap. In this case, $u_{in} = 0$, and Eq. (22) simplifies to

$$0 \approx v_{in}'' + \theta_0 v_{in}' + v_{in}\left(r_2 - \frac{d_2}{\sigma} - r_2 v_{in}\right),$$

exhibiting a tumour wavespeed of

$$\theta \approx 2\sqrt{D}\sqrt{r_2 - \frac{d_2}{\sigma}}. \tag{38}$$

Finally, recalling that the wavefront is fixed at $z = 0$ through translational invariance, we determine the width of the interstitial gap to be given by the location where $u$ attains zero, $z_*$:

$$z_* = \frac{1}{\sqrt{c}} \ln\left(\frac{d_1}{\sigma}\right). \tag{39}$$

We now have a comprehensive picture of the parameter space belonging to Eqs. (7)–(9), and the types of behaviours that can arise within this space, shown in Fig. 5.

Comparing our analytical solutions—Eqs. (35)–(39)—with estimates measured from our numerical solutions (described in Section 3), we see good agreement (Fig. 6). Discrepancies on the order of our asymptotic parameter, $\epsilon$, arise due to our use of leading-order approximations in the asymptotics, but the correspondence is sufficiently close that we do not consider it necessary to include higher-order terms.

To understand the behaviour of Eqs. (35)–(39), we view the 'aggressiveness' of a tumour in terms of the values of its competitive strength and acid-mediated death parameters ($d_2$ and $a_2$, respectively) relative to those of the healthy population ($d_1$ and $a_1$, respectively). We consider 'low' aggressiveness to mean that the tumour death rate and competitive strength parameters are similar to those for the healthy tissue; 'moderate' aggressiveness to indicate a tumour with a death rate approximately half, and competitive strength twice, the values for the healthy tissue; and 'high' aggressiveness to mean a tumour with a death rate an order of magnitude lower, and competitive strength an order of magnitude higher, than those of the healthy tissue.

Under these three aggressiveness characterisations, we vary the healthy cell death rate and competitive strength parameters ($d_1$ and $a_1$, respectively) and plot the resulting

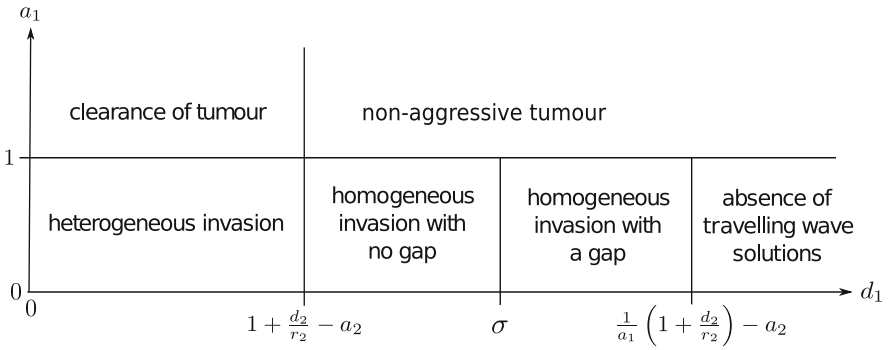


**Fig. 5** A comprehensive schematic of the parameter space and possible behaviours arising from Eqs. (7)–(9), with the additional, biologically motivated, constraint in all regimes that $d_2 \leq d_1$ to capture tumour capacity for acid resistance. In the regime labelled 'absence of travelling wave solutions' we have complicated solutions that do not exhibit travelling waves, stemming from a negative value of $\lambda$ in the exponentially decaying approximation for the acid profile (see Sect. 4.2)

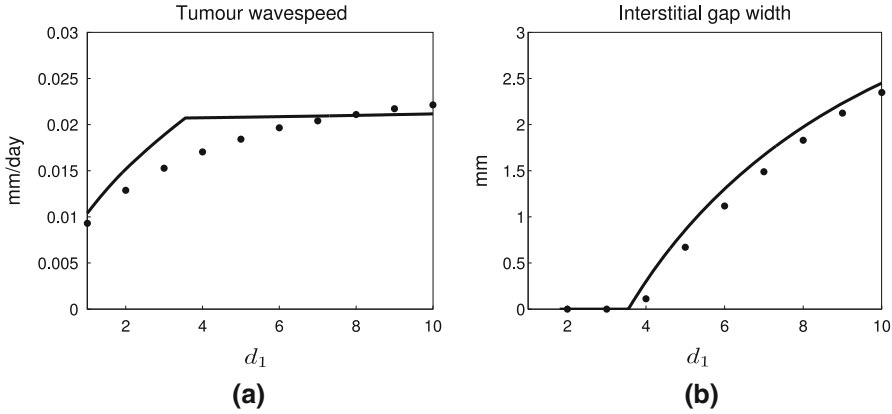


**Fig. 6** Comparison of **a** invasive tumour wavespeeds and **b** interstitial gap widths produced by our analysis from Sect. 4 (*curves*) and numerical simulations detailed in Sect. 3 (*dots*), over increasing rates of acid-mediated healthy cell death, $d_1$, from $d_1 = 1$ to $d_1 = 10$. Other parameters are held constant at $r_2 = 1$, $d_2 = 1$ (maintaining $d_1 \geq d_2$ as required from Sect. 2), $D = 4{\cdot}10^{-5}$, $c = 70$, $a_1 = 0.1$, and $a_2 = 0.2$. Errors of $\mathcal{O}(\epsilon)$ in the analytical curves arise due to our use of leading-order approximations in the asymptotics

wavespeeds (Fig. 7). Broadly speaking the wavespeeds increase with tumour aggressiveness as one would expect. Increasing aggressiveness also compresses the regime of valid travelling wave solutions, as a result of the parameter condition in Eq. (31), which when violated produces a complex solution for the acid profile (see Sect. 4.2).

Returning to the interstitial gap, we again vary the healthy death and competition parameters under three degrees of tumour aggressiveness, but plot interstitial gap width rather than wavespeed (Fig. 8). We find that gap width increases with aggressiveness, from no gaps in much of the parameter space for 'low' aggressiveness to gaps as large as 5 mm in the parameter space for 'high' aggressiveness. To be realistic, however, interstitial gaps must fulfil two criteria. First, their size must fall within the range

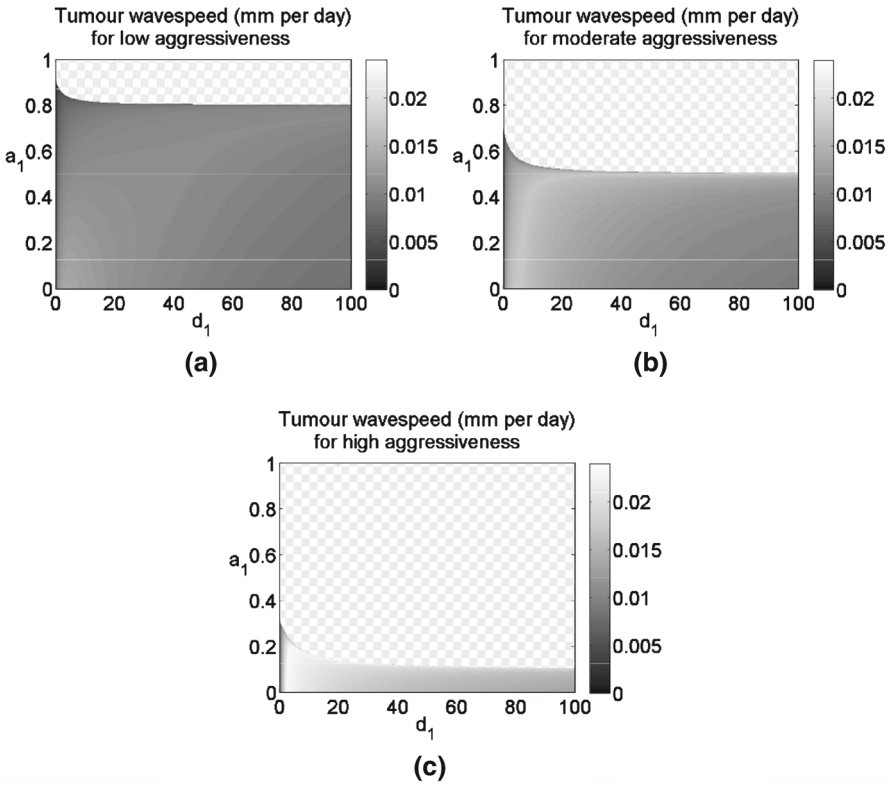


**Fig. 7** Effect of tumour aggressiveness on the speed of invasion. Tumour wavespeed, as found in Sect. 4.3, is plotted (greyscale gradients, redimensionalised to millimetres per day) by healthy death rate ($d_1$) and healthy competitive strength ($a_1$) on the $x$ and $y$ axes, respectively. The checkered regions mark parameter combinations that are outside the regime of travelling wave solutions. **a** The tumour acid-mediated death rate ($d_2$) is set to $0.8d_1$ and tumour competitive strength ($a_2$) to $1.2a_1$, representing tumours which are only mildly aggressive; **b** $d_2$ is set to $0.5d_1$ and $a_2$ to $2a_1$, representing moderately aggressive tumours; **c** $d_2$ is set to $0.1d_1$ and $a_2$ to $10a_1$, representing highly aggressive tumours. Other parameters are held constant at $r_2 = 1$, $D = 4 \cdot 10^{-5}$, and $c = 70$

observed experimentally by Gatenby and Gawlinski; that is, on the order of 0.1 mm (Gatenby and Gawlinski 1996). Second, the tissue pH established inside the tumour, which comes from our solution for $w$ near the core, must be experimentally plausible; the core was assumed *a priori* to be non-necrotic (Gatenby and Gawlinski 1996), and hence the pH must be higher (less acidic) than 6.3, the commonly observed threshold for tumour cell survival (Park et al. 1999). Taking these two criteria together, it emerges that while gaps in general arise over a large portion of parameter space, *realistic* gaps occur in a fairly restricted space that shrinks as the aggressiveness of the tumour increases, indicating that realistic gaps are sensitive to parameter choice.

Finally, some past experiments have indicated a lack of correlation between speed of invasion and the density of healthy cells, stroma, and other material mixed in with the tumour (Dvorak et al. 1983). Sampling our $(a_1, a_2, d_1, d_2)$ parameter space while holding all other parameters constant reveals the presence of a negative correlation

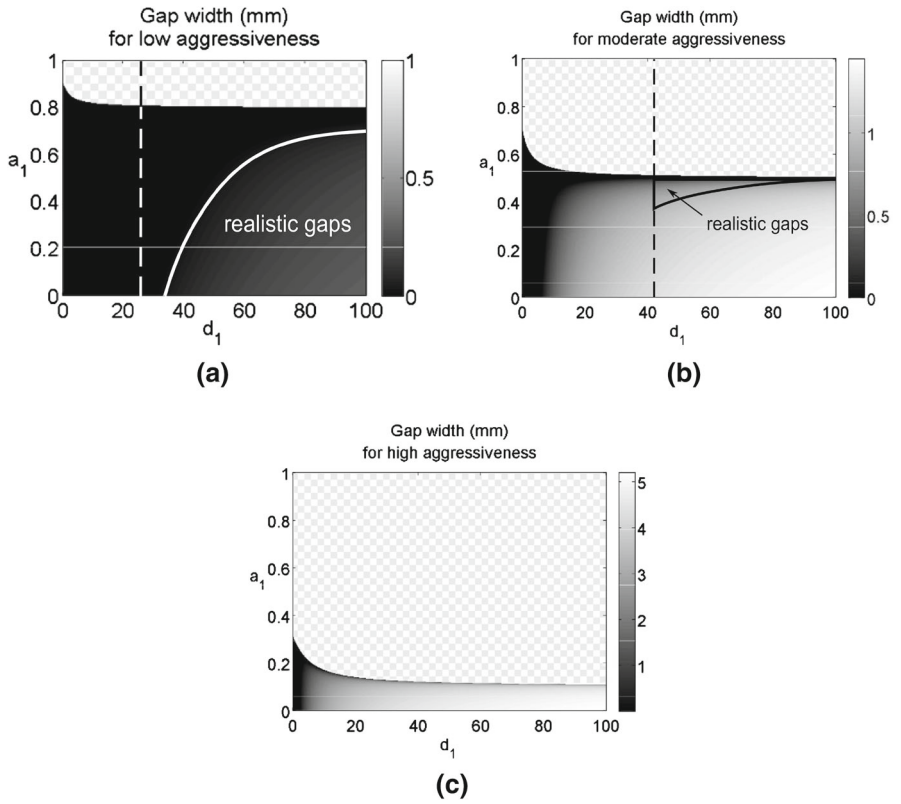


**Fig. 8** Effect of tumour aggressiveness on the width of the interstitial gap and parameter spaces giving rise to realistic gaps. Interstitial gap width, as found in Sect. 4.3, is plotted (greyscale gradients, redimensionalised to millimetres) by healthy death rate ($d_1$) and healthy competitive strength ($a_1$) on the $x$ and $y$ axes, respectively, with the checkered regions marking parameter combinations that are outside the regime of travelling wave solutions. **a** Tumour acid-mediated death rate ($d_2$) is set to $0.8d_1$ and tumour competitive strength ($a_2$) to $1.2a_1$, representing tumours which are only mildly aggressive; **b** $d_2$ is set to $0.5d_1$ and $a_2$ to $2a_1$, representing moderately aggressive tumours; **c** $d_2$ is set to $0.1d_1$ and $a_2$ to $10a_1$, representing highly aggressive tumours. The *dashed lines*, *white* on **a** and *black* on **b**, represent the threshold pH value of 6.3, below which tumours are not seen clinically (Park et al. 1999). To the *right* of each of these *dashed lines*, the tissue pH near the tumour core—calculated by converting the acid profile ($w$) near the left-hand domain boundary to pH units—is above this threshold, meaning it is clinically plausible. In **c** the pH is lower than the threshold of 6.3, and hence unrealistic, for all parameter choices. Gap widths on the order of 0.1 mm are within the range observed experimentally in Gatenby and Gawlinski (1996); allowing widths of up to 1 mm, and incorporating the pH information, the regions of parameter space giving rise to biologically realistic interstitial gaps are outlined by the *solid curves*, *white* in **a** and *black* in **b**. Despite the occurrence of gaps ranging to 5 mm in width in **c**, none of the gaps are realistic due to the implausibly low pH values. In all three figures, the fixed parameters are $r_2 = 1$, $D = 4 \cdot 10^{-5}$, and $c = 70$

between wavespeed and healthy density (Fig. 9a); and a positive non-linear correlation between wavespeed and tumour density, albeit with considerable spread (Fig. 9b).

In the following section we discuss some implications of the analytical results presented here and future directions to which they lead.

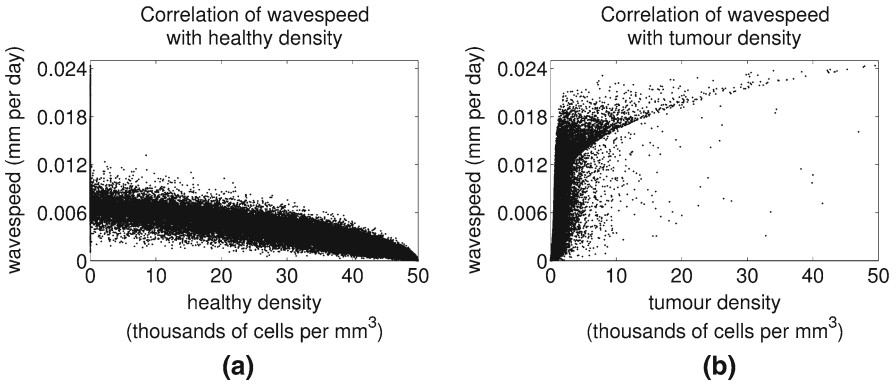


**Fig. 9** Correlation between invasive speed and density of cells remaining behind the advancing front, obtained by taking $10^5$ random samples from uniform distributions of $a_1$, $a_2$, $d_1$, and $d_2$ in the invasive regimes, subject to the ranges and biologically motivated constraints listed in Table 2 (with the remaining parameters held constant at $r_2 = 1$, $D = 4 \cdot 10^{-5}$, and $c = 70$), and applying the results from Sect. 4. **a** Tumour wavespeed, in millimetres per day, is plotted against the density of healthy cells near the core, in thousands of cells per cubic millimetre. **b** Tumour wavespeed is plotted against the density of tumour cells near the core, with the same units as in **a**. The tissue carrying capacity for both cell types is 50 thousand cells per cubic millimetre

## 5 Discussion

We have incorporated additional, potentially important, biological features into the canonical Gatenby–Gawlinski model of acid-mediated invasion to generalise its descriptive power beyond the highly aggressive cases considered in Gatenby and Gawlinski (1996) (Sect. 2). By rendering the healthy state conditionally stable rather than globally unstable, we have obtained four tumour behaviours, two of which are non-invasive or non-aggressive and were not captured by the original model (Sect. 3, Fig. 3). We would caution, however, against translating these non-invasive and non-aggressive cases directly to an *in vivo* or clinical setting, not least because competitive strength of the healthy population ($a_1$) is a somewhat abstract term and finding a one-to-one correspondence between it and an adjustable property of the biological system may prove difficult. Nevertheless, it is promising that we have attained such behaviours, in part because they may provide good targets for model validation. In this respect our model fits into a larger goal of assessing possible experiments that will test the acid-mediated invasion hypothesis, an important task in light of novel treatment strategies, such as buffering therapy (Robey et al. 2009; Silva et al. 2009; Martin et al. 2010, 2011; Alfarouk et al. 2011; Robey and Martin 2011), to which the hypothesis has given rise.

Furthermore, Sect. 4 demonstrates that our model remains amenable to mathematical analysis. Through an asymptotic travelling wave analysis we have fully characterised the invasive behaviours in the parameter space, finding these to be consistent both with our own numerical solutions (Fig. 6) and with previous mathematical and experimental descriptions of the system (Gatenby and Gawlinski 1996; Fasano et al. 2009). It should be noted that existence of the minimum wavespeed has not been

proven here, and this remains a general open problem for travelling wave systems with multiple species. Our numerical simulations indicate, however, that the minimum wavespeed is indeed established, at least for the parameter ranges we have considered. Taking all of this together, we suggest that our general model, which captures more biologically observed phenomena than the original Gatenby–Gawlinski model while preserving its structural stability and key results, may be useful for further targeted studies of the kind seen in Martin et al. (2010) or McGillen et al. (2012).

Our finding that the interstitial gap is sensitive to parameter choice (Fig. 8) leads to the modelling prediction that the gap is perhaps unlikely to be a widespread feature of tumour invasion. This finding is not inconsistent with the experimental results in Gatenby and Gawlinski (1996), in which the formation of hypocellular interstitial gaps along the tumour–host interfaces was observed in 14 out of 21 fixed specimens. We note that our model predicts gaps in mildly aggressive tumours rather than the highly aggressive tumours predicted by the Gatenby–Gawlinski formulation, most likely due to our inclusion of the biologically realistic, but aggression-limiting, features of tumour cell death and cellular competition, as well as our experimentally-motivated lower limit on tissue pH. In future the mathematical results presented herein should be supplemented by experiments to pin down the range of permissible widths for the gap and determine its comparative frequency of occurrence in, for example, fixed versus unfixed *in vitro* specimens. Moreover, as gaps observed experimentally in Gatenby and Gawlinski (1996) are on roughly the scale of a single cell, it is probable that stochastic effects play a role in their formation, and a discrete realisation of Eqs. (7)–(9) could help to evaluate whether gaps could be, for example, a transient feature of tumour invasion.

Lastly, the correlations we have found between invasive speed and cell densities inside the tumour (Fig. 9) are at odds with past experimental results that saw no such correlations (Dvorak et al. 1983), indicating that something more must be influencing the system dynamics than we have considered here. While the Gatenby–Gawlinski model was an elegant first investigation into the acid-mediated invasion hypothesis, and the generalisation presented in this paper provides a formulation applicable to a wider variety of tumour scenarios, both are coarse-grained descriptions of the tissue-scale dynamics. It is likely, though, that tissue-scale consequences of the Warburg Effect emerge from the intricate biochemical mechanisms by which tumour cells handle their metabolically-derived intracellular acid loads and govern the spatial coordination of their intracellular pH; hence, a finer-scale understanding of tumour pH may be necessary for true insight into acid-mediated invasion. Such an understanding would have immediate implications for buffering therapy and perhaps could point the way to treatment strategies not yet considered.

**Acknowledgments** JBM, NKM, and PKM were partially supported by the National Cancer Institute, National Institutes of Health grant U54CA143970. JBM was partially supported by an Overseas Graduate Scholarship from St. Catherine's College at Oxford University and would like to thank the Systems Biology Doctoral Training Centre for its hospitality. NKM and PKM were partially supported by the National Cancer Institute, National Institutes of Health grant U56CA113004. PKM was partially supported by a Royal Society Wolfson Research Merit award. This work is produced by NKM under the terms of the postdoctoral research training fellowship issued by the NIHR. The views expressed in this publication are those of the authors and not necessarily those of the NHS, The National Institute for Health Research or the Department of Health.

## References


Alfarouk KO, Muddathir AK, Shayoub MEA (2011) Tumor acidity as evolutionary spite. Cancers 3(1):408–414

Basanta D, Ribba B, Watkin E, You B, Deutsch A (2010) Computational analysis of the influence of microenvironment on carcinogenesis. Math Biosci 229:22-29

Bender CM, Orszag SA (1999) Advanced mathematical methods for scientists and engineers I: asymptotic methods and perturbation theory. Springer, New York

Bertuzzi A, Fasano A, Gandolfi A, Sinisgalli C (2010) Necrotic core in EMT6/Ro tumour spheroids: is it caused by an ATP deficit? J Theor Biol 262:142–150

Bianchini L, Fasano A (2009) A model combining acid-mediated tumour invasion and nutrient dynamics. Nonlinear Anal Real World Appl 10(4):1955–1975

Byrne HM (2010) Dissecting cancer through mathematics: from the cell to the animal model. Nat Rev Cancer 10:221–230

Casciari JJ, Sotirchos SV, Sutherland RM (1992) Variations in tumor cell growth rates and metabolism with oxygen concentration, glucose concentration, and extracellular pH. J Cell Physiol 151(2):386–394

Clarke R, Dickson RB, Bruenner N (1990) The process of malignant progression in human breast cancer. Annals Oncol 1(6):401–407

Dale PD, Sherratt JA, Maini PK (1994) Mathematical modeling of corneal epithelial wound healing. Math Biosci 124(2):127–147

DeBerardinis RJ, Lum JJ, Hatzivassiliou G, Thompson CB (2008) The biology of cancer: metabolic reprogramming fuels cell growth and proliferation. Cell Metabol 7:11–20

Dvorak HF, Senger DR, Dvorak AM (1983) Fibrin as a component of the tumor stroma: origins and biological significance. Cancer Metastasis Rev 2(1):41–73

Fasano A, Herrero MA, Rodrigo MR (2009) Slow and fast invasion waves in a model of acid-mediated tumour growth. Math Biosci 220(1):45–56

Fidler IJ, Hart IR (1982) Biological diversity in metastatic neoplasms: origins and implications. Science 217(4564):998–1003

Gatenby RA (1991) Population ecology issues in tumor growth. Cancer Res 51(10):2542–2547

Gatenby RA, Gawlinski ET (1996) A reaction-diffusion model of cancer invasion. Cancer Res 56(24):5745–5753

Gatenby RA, Gillies RJ (2004) Why do cancers have high aerobic glycolysis? Nat Rev Cancer 4(11):891–899

Gatenby RA, Smallbone K, Maini PK, Rose F, Averill J, Nagle RB, Worrall L, Gillies RJ (2007) Cellular adaptations to hypoxia and acidosis during somatic evolution of breast cancer. British J Cancer 97(5):646–653

Gillies RJ, Gatenby RA (2007) Hypoxia and adaptive landscapes in the evolution of carcinogenesis. Cancer Metastasis Rev 26(2):311–317

Gillies RJ, Verduzco D, Gatenby RA (2012) Evolutionary dynamics of cancer and why targeted therapy does not work. Nat Rev Cancer 12:487–493

Hanahan D, Weinberg RA (2011) Hallmarks of cancer: the next generation. Cell 144:646–674

Kallinowski F, Vaupel P, Runkel S, Berg G, Fortmeyer HP, Baessler KH, Wagner K, Mueller-Klieser W, Walenta S (1988) Glucose uptake, lactate release, ketone body turnover, metabolic micromilieu, and pH distributions in human breast cancer xenografts in nude rats. Cancer Res 48(24):7264–7272

Kroemer G, Pouyssegur J (2008) Tumor cell metabolism: cancer's Achilles' heel. Cancer Cell 13:472–482

Lide D (1994) CRC handbook of chemistry and physics (student's 73rd revised ed.). CRC Press, Boca Raton

Martin GR, Jain RK (1994) Noninvasive measurement of interstitial pH profiles in normal and neoplastic tissue using fluorescence ratio imaging microscopy. Cancer Res 54(21):5670–5674

Martin NK, Gaffney EA, Gatenby RA, Maini PK (2010) Tumour-stromal interactions in acid-mediated invasion: a mathematical model. J Theor Biol 267(3):461–470

Martin NK, Gaffney EA, Gatenby RA, Gillies RJ, Robey IF, Maini PK (2011) A mathematical model of tumour and blood pHe regulation: the HCO3-/CO2 buffering system. Math Biosci 230(1):1–11

McCarthy N (2009) Metabolism: room to breathe. Nat Rev Cancer 9:13

McGillen JB, Martin NK, Robey IF, Gaffney EA, Maini PK (2012) Applications of mathematical analysis to tumour acidity modelling. U. Kyoto RIMS Kôkyûroku Bessatsu B31:31–59

Murray JD (2002) Mathematical biology: I. An introduction. Interdisciplinary applied mathematics. 3rd edn. Springer, New York
Nieweg OE, Pruim J, Vaalburg W (1996) Fluorine-18-fluorodeoxyglucose PET imaging of soft-tissue sarcoma. J Nucl Med 37:257–261
Nowell PC (1976) The clonal evolution of tumor cell populations. Science 194(4260):23–28
Park HJ, Lyons JC, Ohtsubo T, Song CW (1999) Acidic environment causes apoptosis by increasing caspase activity. British J Cancer 80(12):1892–1897
Pienta KJ, McGregor N, Axelrod R, Axelrod DE (2008) Ecological therapy for cancer: defining tumors using an ecosystem paradigm suggests new opportunities for novel cancer treatments. Transl Oncol 1(4):158–164
Robey IF, Martin NK (2011) Bicarbonate and dichloroacetate: evaluating pH altering therapies in a mouse model for metastatic breast cancer. BMC Cancer 11:235–245
Robey IF, Baggett BK, Kirkpatrick ND, Roe DJ, Dosescu J, Sloane BF, Hashim AI, Morse DL, Raghunand N, Gatenby RA, Gillies RJ (2009) Bicarbonate increases tumor pH and inhibits spontaneous metastases. Cancer Res 69(6):2260–2268
van Saarloos W (1988) Front propagation into unstable states: marginal stability as a dynamical mechanism for velocity selection. Phys Rev A 37(1):211–229
Schiesser WE (1991) The numerical method of lines: integration of partial differential equations. 1st edn. Academic Press, San Diego
Silva AS, Yunes JA, Gillies RJ, Gatenby RA (2009) The potential role of systemic buffers in reducing intratumoral extracellular pH and acid-mediated invasion. Cancer Res 69(6):2677–2684
Smallbone K, Gavaghan D, Gatenby RA, Maini PK (2005) The role of acidity in solid tumour growth and invasion. J Theor Biol 235(4):476–484
Tracqui P, Cruywagen GC, Woodward DE, Bartoo GT, Alvord EC, Murray JD (1995) A mathematical model of glioma growth: the effect of chemotherapy on spatio-temporal growth. Cell Prolif 28(1):17–31
Venkatasubramanian R, Henson MA, Forbes NS (2006) Incorporating energy metabolism into a growth model of multicellular tumor spheroids. J Theor Biol 242:440–453
Vogelstein B, Fearon ER, Hamilton SR, Kern SE, Preisinger AC, Leppert M, Smits AM, Bos JL (1988) Genetic alterations during colorectal-tumor development. New Engl J Med 319(9):525–532
Warburg O (1930) The metabolism of tumors. Arnold Constable, London
Warburg O (1956) On the origin of cancer cells. Science 123:309–314